Helical locomotion in a porous medium

Ye Chen, Noah Lordi, Michael Taylor, and On Shun Pak* Department of Mechanical Engineering, Santa Clara University, Santa Clara, California 95053, USA

(Received 5 August 2020; accepted 6 October 2020; published 28 October 2020)

Microorganisms and artificial microswimmers often need to swim through environments that are more complex than purely viscous liquids in their natural habitats or operational environments, such as gel-like mucus, wet soil, and aquifers. The question of how the properties of these complex environments affect locomotion has attracted considerable recent attention. In this paper, we present a theoretical model to examine how the additional resistance due to the network of stationary obstacles in a porous medium affects helical locomotion. Here, we focus on helical locomotion for its ubiquity as a propulsion mechanism adopted by many swimming bacteria and artificial microswimmers. We show that the additional resistance can have qualitatively different effects on various scenarios of helical locomotion: (1) a helical propeller driven by an external torque, (2) a free swimming bacterium consisting of a helical flagellum and a head, and (3) a cargo-carrying helical propeller driven by an external torque. Our results elucidate the subtle and significant differences between torqued helical propulsion versus force-free and torque-free swimming in a porous medium. We also remark on the limitations as well as potential connections of our results with experimental measurements of bacterial swimming speeds in polymeric solutions.

DOI: 10.1103/PhysRevE.102.043111

I. INTRODUCTION

Locomotion of microorganisms is critical for various biological functions, including reproduction, foraging, and escaping from predators [1-3]. The Reynolds number (Re), which characterizes the inertial to viscous forces, of their locomotion typically ranges from 10⁻⁵ for swimming bacteria to 10^{-2} for human spermatozoa [4,5]. Inertial effects are therefore virtually absent in this regime, imposing stringent constraints on effective locomotion strategies at low Re. For instance, Purcell's scallop theorem rules out any reciprocal motion (motion with time-reversal symmetry) for self-propulsion in the absence of inertia [6]. Microorganisms exploit different mechanisms to escape the constraints from the scallop theorem. The past decades have seen tremendous progress in understanding the physical principles underlying the locomotion of swimming microorganisms [3-9]. In parallel, substantial interdisciplinary efforts have also led to the development of artificial microswimmers, which have demonstrated great promise for biomedical and environmental applications, such as targeted drug delivery, microsurgery, and environmental remediation [10–16].

Earlier works typically assumed the medium surrounding the microswimmers to be a purely viscous liquid. However, both microorganisms and artificial microswimmers often need to move through complex heterogeneous environments in their natural habitats or operational environments, such as gastric and cervical mucus, soils, and aquifers [17,18]. The question of how the complex properties of the surrounding medium affect the swimming performance has attracted considerable recent attention [19,20]. Motivated by the locomotion of microorganisms in porous media (e.g., wet soils and aquifers) for applications including environmental remediation and enhanced oil recovery [14], we focus here on the effect due to a matrix of stationary obstacles (such as fibers or grains) embedded into a purely viscous solvent on locomotion. The relevance of such a physical scenario for the movement of microorganisms through biological filamentous media such as gel-like mucus and extracellular matrix has also been suggested [17,18,21]. Previous work in this area has captured the indirect, viscous solvent-mediated interactions between a swimmer and its surrounding obstacles by an effective medium approach [17,21,22]. These interactions can be captured by solving the properly averaged (mean-field) equation describing the viscous, incompressible flow through a random, sparse network of stationary obstacles given by the Brinkman equation [23–26],

$$-\nabla p + \mu \nabla^2 \mathbf{u} = \mu \alpha^2 \mathbf{u}, \quad \nabla \cdot \mathbf{u} = 0. \tag{1}$$

Here \mathbf{u} and p are, respectively, the average velocity and pressure fields, μ is the dynamic viscosity, and α^{-2} is the permeability. The Stokes equation is recovered in the limit when $\alpha = 0$; the term $\mu \alpha^2 \mathbf{u}$ represents additional resistance due to the network of stationary obstacles. The validity of the Brinkman equation at low particle volume fraction was established by proper averaging methods [23–26]. At larger volume fractions, the Brinkman equation is not expected to be quantitatively accurate, but the approximation may still be effective in capturing the qualitative behavior [27]. Such an effective medium approach via the Brinkman equation has been applied to model different types of swimmers in porous media [18,28-32].

^{*}opak@scu.edu

In this paper, we focus on helical locomotion for its ubiquity as a propulsion mechanism adopted by many swimming bacteria [3,33,34] and artificial microswimmers [35–38]. Bacteria such as Escherichia coli and Vibrio alginolyticus employ relatively rigid helical flagella for self-propulsion. These bacterial flagella are helical filaments connected to the cell body via a rotary motor, which drives the rotation of the helical flagella to generate propulsion [4,39,40]. Bacterial locomotion has inspired the design of artificial helical propellers, which are magnetic helical microstructures resembling bacterial flagella. Instead of being driven by the rotary motor embedded in the cell membrane of a bacterium, artificial helical propellers are driven by external torques imposed by rotating magnetic fields. While the former scenario results in a swimming bacterium that is force-free and torque-free, artificial helical propellers are not torque-free but torqued by the external magnetic field. This subtle difference could lead to qualitatively different effects on propulsion performance in a purely viscous liquid [41] and in a porous medium as shown later in this paper.

The pioneering work by Leshansky [17] analyzed the propulsion of a rotating helix and found faster propulsion speeds with increased resistance in a Brinkman medium than in a purely viscous liquid. Here we extend the analysis to consider a full model for a bacterium consisting of a helical flagellum and a cell body (head) swimming in a porous medium. The presence of the head is essential in realizing a force-free and torque-free swimming bacterium as elucidated by Chwang and Wu [41]. Compared with the case of a rotating helix, the inclusion of the head in the bacterium model modifies the physical picture in two ways: The first obvious effect is that the head contributes additional drag on the overall structure, hindering its propulsion. The second effect, more subtle, is that the rotation of the helical flagellum will induce counter-rotation of the entire bacterium (head plus the flagellum) to balance the torque from the flagellum for the bacterium to remain torque-free. Without a head, the only way for a rotating helix to maintain torque-free motion is to counter-rotate at exactly the same speed but in the opposite direction, effectively canceling all propulsive thrust and thus leading to zero propulsion [41]. These two competing effects give rise to some optimal head sizes that maximize the speed of a swimming bacterium. We extend the analyses by Chwang and Wu in a purely viscous liquid to probe the effect of additional resistance in a Brinkman medium on bacterial locomotion, when the subtle and crucial dynamics of the head is included in the analysis. In contrast to previous conclusions on a rotating helix [17], our results show that the additional resistance can have both quantitatively and qualitatively different effects on various types of helical locomotion in porous media.

The paper is organized as follows. We formulate the problem in Sec. II by introducing the swimmer model (Sec. II A) and the description of its dynamics in a porous medium (Sec. II B). In Sec. III, we first reproduce previous results on a rotating helical propeller driven by an external torque in a porous medium [17] (Sec. III A), before considering a force-free and torque-free model for a swimming bacterium (Sec. III B). We then elucidate the difference in the dynamics of a swimming bacterium and a cargo-carrying helical pro-

peller driven by an external torque in Sec. III C, before some concluding remarks in Sec. IV.

II. FORMULATION

A. Swimmer model

We first describe the setup shown in Fig. 1 as a model for a swimming bacterium. The same geometrical setup applies to other types of helical locomotion (i.e., artificial helical propellers with and without a cargo) considered in this paper with modifications explained later. The model consists of a spherical head of radius R and a helically shaped flagellum with centerline $\mathbf{r} = r \cos[kz + (\omega - \Omega)t]\mathbf{e}_x + r \sin[kz + \omega]\mathbf{e}_x + r \cos[kz + \omega$ $(\omega - \Omega)t]\mathbf{e}_v + (z + Ut)\mathbf{e}_z$. Here r is the helix radius, k is the wave number, $z = s/\sqrt{1 + r^2k^2}$, θ is the pitch angle with $\tan \theta = rk$, N is the number of helical turns, U is the undetermined swimming speed, and s and t are the arc length and time, respectively. We have followed the analysis by Chwang and Wu [41] and assumed unidirectional swimming and rotation in the z direction here. A full three-dimensional analysis can be similarly performed following the analysis by Keller and Rubinow [42]. When the helical flagellum is rotated by the motor at its base at a given rate $\omega \mathbf{e}_z$, the flagellum not only generates a propulsive thrust but also a torque about the z axis. This torque induces the entire swimmer (the head plus the flagellum) to counter-rotate at an undetermined rate $-\Omega \mathbf{e}_{z}$. Therefore, the helical flagellum rotates at an apparent rate $(\omega - \Omega)\mathbf{e}_z$, while the head rotates in the opposite direction at the rate $-\Omega \mathbf{e}_z$ (Fig. 1). The goal of the following calculation is to determine the unknown translational ($\mathbf{U} = U\mathbf{e}_{\tau}$) and rotational ($\Omega = -\Omega \mathbf{e}_z$) velocities of a swimming bacterium in a porous medium.

B. Dynamics in a porous medium

We use the same framework based on the resistive force theory (RFT) by Leshansky [17] to describe the dynamics of the flagellum in a porous medium modeled by the Brinkman equation [Eq. (1)]. Similar to the RFT in a purely viscous liquid, the force density \mathbf{f} on the flagellum depends only on the local velocity $\mathbf{u} = d\mathbf{r}/dt$ as

$$\mathbf{f} = -[\xi_{\perp}(\mathbf{I} - \mathbf{t}\mathbf{t}) + \xi_{\parallel}\mathbf{t}\mathbf{t}] \cdot \mathbf{u}, \tag{2}$$

where $\mathbf{t} = d\mathbf{r}/ds$ is the local tangent vector, \mathbf{I} is the identity tensor, and the resistive coefficients ξ_{\perp} and ξ_{\parallel} characterize, respectively, the force densities due to transverse and axial

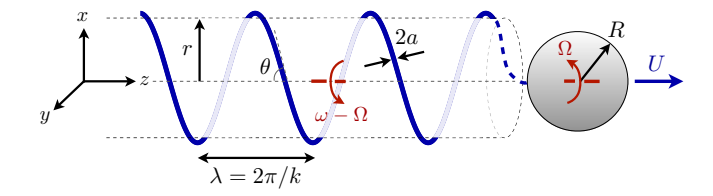


FIG. 1. Notations and geometrical setup of the model of a swimming bacterium consisting of a spherical head and a helically shaped flagellum.

translation of a straight cylinder. In a Brinkman medium, the coefficients are given by [17,43]

$$\frac{\xi_{\perp}}{4\pi\,\mu} = \frac{1}{4}(a\alpha)^2 + a\alpha\frac{K_1(a\alpha)}{K_0(a\alpha)},\tag{3}$$

$$\frac{\xi_{\parallel}}{4\pi\,\mu} = \frac{1}{2}a\alpha \frac{K_1(a\alpha)}{K_0(a\alpha)},\tag{4}$$

where K_p are the modified Bessel functions of degree p. The drag anisotropy measured by the ratio $\gamma = \xi_{\perp}/\xi_{\parallel} = 2 +$ $\alpha a K_0(\alpha a)/[2K_1(\alpha a)]$ is essential to the generation of propulsive thrust in flagellar swimming [5]. The effectiveness of this RFT approach in a Brinkman medium was demonstrated by validations against numerical simulations that explicitly model the porous medium as random arrays of stationary spheres [17]. However, special attention is required in the limit of vanishing resistance $a\alpha \to 0$ as noted in Ref. [17]: while the drag anistropy ratio reduces to the value in the Stokes limit ($\gamma = 2$), the individual coefficients do not recover their corresponding values in this limit due to its singular nature. Moreover, biologically relevant values of the scaled resistance $a\alpha$ in filamentous media are typically estimated to be of O(0.1)-O(1) or higher [17,28,30,44]. We therefore focus on results for $a\alpha \ge 0.1$ in the main text and only remark on some interesting observations for smaller values of $a\alpha$ in the Appendix.

In addition to the flagellar dynamics, the additional resistance in a Brinkman medium also alters the translational and rotational dynamics of the head. The hydrodynamic force $(\mathbf{F}_h = -6\pi \mu R \mathbf{U} C_f)$ and torque $(\mathbf{T}_h = -8\pi \mu R^3 \mathbf{\Omega} C_t)$ acting on the spherical head are modified, with the correction factors given by [17,45]

$$C_f = 1 + R\alpha + \frac{R^2\alpha^2}{9},\tag{5}$$

$$C_t = 1 + \frac{R^2 \alpha^2}{3(1 + R\alpha)}.$$
(6)

We remark that when the separation between the obstacles in the porous medium is small compared with a characteristic length scale of the swimmer (i.e., $a\alpha \gg 1$ or $R\alpha \gg 1$), the above results based on the Brinkman medium approach is not expected to be quantitatively accurate and may only capture the dynamics qualitatively [27].

For locomotion at low Re, the overall force-free and torque-free conditions, respectively, read

$$\int_0^L \mathbf{f} \ ds + \mathbf{F}_h = \mathbf{0},\tag{7}$$

$$\int_0^L \mathbf{r} \times \mathbf{f} \, ds + \mathbf{T}_h = \mathbf{0},\tag{8}$$

where $L = 2\pi N \sqrt{r^2 + (1/k)^2}$ is the length of the flagellum. Under the assumption of undirectional swimming and rotation in the z direction [41], the above force and torque balances therefore reduce to

$$(1 + \gamma \kappa^2 + AC_f)U + (\gamma - 1)\kappa r\Omega = (\gamma - 1)\kappa^2 c, \qquad (9)$$

$$(\gamma - 1)\kappa U + (\gamma + \kappa^2 + BC_t)r\Omega = \kappa(\gamma + \kappa^2)c, \quad (10)$$

respectively, where $A = 3\mu R\kappa \sqrt{1 + \kappa^2}/(N\xi_{\parallel}r)$, $B = 4\mu R^3\kappa \sqrt{1 + \kappa^2}/(N\xi_{\parallel}r^3)$, $c = \omega/k$, $\gamma = \xi_{\perp}/\xi_{\parallel}$, and $\kappa = \tan\theta = rk$. Solving the system of equations [Eqs. (9) and (10)] for U and Ω yields the solution

$$\frac{U}{r\omega} = \frac{BC_t(\gamma - 1)\kappa}{\Delta},\tag{11}$$

$$\frac{\Omega}{\omega} = \frac{\gamma [1 + 2\kappa^2 + \kappa^4 + AC_f(1 + \kappa^2)]}{\Delta},\tag{12}$$

where $\Delta = BC_t(AC_f + 1 + \gamma \kappa^2) + AC_f(\gamma + \kappa^2) + \gamma(1 + 2\kappa^2 + \kappa^4)$. These results extend previous analyses in two ways. First, we extend the analysis by Chwang and Wu on a swimming bacterium in a purely viscous liquid [41] to a porous medium modeled by the Brinkman equation. Second, we also extend the analysis by Leshansky on a rotating helical propeller driven by an external torque in a Brinkman medium [17] to a force-free and torque-free swimming bacterium. We discuss in the next section the quantitative and qualitative changes compared with these previous results.

III. RESULTS AND DISCUSSION

Based on the formulation and results in Sec. II, we consider here different types of helical motion in a porous medium in the following sections: (1) a helical propeller driven by an external torque (Sec. III A), (2) a free swimming bacterium consisting of a helical flagellum and a head (Sec. III B), and (3) a cargo-carrying helical propeller driven by an external torque (Sec. III C).

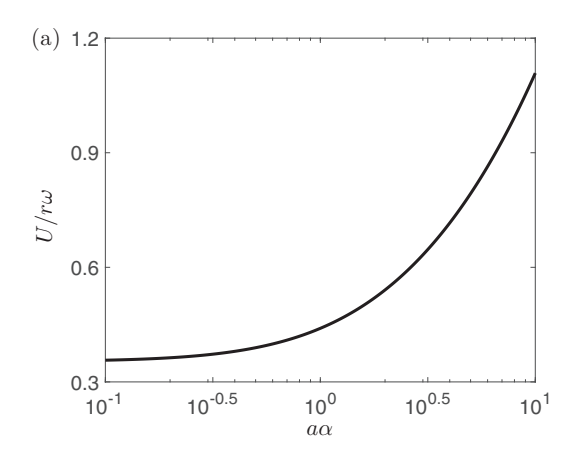
A. A rotating helical propeller driven by an external torque

We first reduce our results to that of a previous analysis of a helical propeller rotating at a prescribed rotation speed ω in a Brinkman medium [17]. Since the rotating helix is driven by an external torque (i.e., not torque-free), we only need to enforce the force-free condition [Eq. (9)] and set the size of the sphere R=0 to determine the resulting propulsion speed U as

$$\frac{U}{r\omega} = \frac{(\gamma - 1)\kappa}{1 + \gamma\kappa^2},\tag{13}$$

where the drag anisotropy ratio is given by $\gamma = \xi_{\perp}/\xi_{\parallel} = 2 + \alpha a K_0(\alpha a)/[2K_1(\alpha a)] \geqslant 2$ in the Brinkman medium. We note that, for all values of α , the ratio γ is greater than that in a purely viscous liquid, where $\gamma = 2$ for very slender filaments [5]. Since anisotropic drag is essential to the generation of propulsive thrust for slender bodies [5], for the same rotational speed, the greater drag anistropy in a Brinkman medium leads to faster propulsion speed in a Brinkman medium than in a purely viscous liquid. Moreover, for a given value of resistance α in a Brinkman medium, there exists an optimal pitch angle of the helix θ that maximizes its propulsion speed. It can be determined from Eq. (13) that the optimal pitch angle occurs at $\tan \theta = 1/\sqrt{\gamma}$, where the corresponding swimming speed is given by

$$\frac{U}{r\omega} = \frac{\gamma - 1}{2\sqrt{\gamma}}. (14)$$



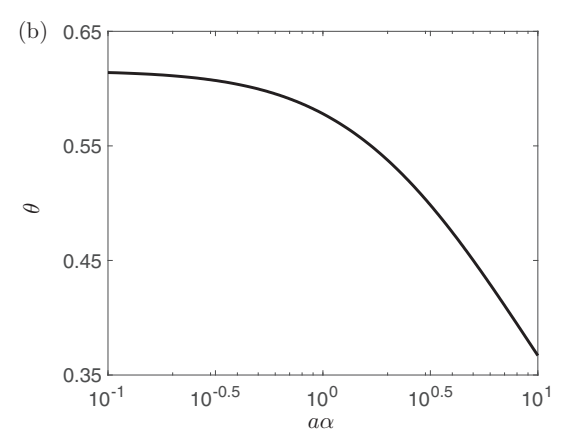


FIG. 2. Propulsion of a rotating helical propeller driven by an external torque in a Brinkman medium. (a) The scaled propulsion speed, $U/r\omega$, as a function of the scaled resistance $a\alpha$. For each value of the scaled resistance, the speed is optimized over the pitch angle, θ . The corresponding optimal values of θ are shown in (b). The results are the same as that given by Leshansky [17].

Figure 2(a) shows that the scaled optimal swimming speed $U/(r\omega)$ increases monotonically with the scaled resistance αa in a Brinkman medium. The corresponding optimal pitch angle θ is shown in Fig. 2(b). The calculation here reproduces the conclusion that the propulsion of a rotating helical propeller is enhanced in a Brinkman medium [17]. As a remark, a similar behavior is observed for smaller values of the scaled resistance [17] as discussed in the Appendix.

B. A swimming bacterium consisting of a helical flagellum and a head

In Sec. III A, the helical propeller is driven to rotate at a prescribed rotation speed by an external torque. The torque-free condition [Eq. (10)] therefore does not apply to this case; instead, the net hydrodynamic torque acting on the helix is equal to the external torque required to drive the rotation at the prescribed rate. Since a swimming bacterium is both force-free and torque-free, the model in Sec. III A is more appropriate for a magnetically driven artificial helical propeller but not a free swimming bacterium.

As elucidated by Chwang and Wu [41], to satisfy the torque-free condition, it is essential to include the head of the bacterium in the analysis (see Introduction, Sec. I). The head is induced to counter-rotate and generate the torque required to balance the torque due to the rotating flagellum. A swimming bacterium with a vanishingly small head cannot swim effectively due to the absence of the counterbalancing torque from the head. In such case, the torque-free condition would induce the flagellum to counter-rotate at virtually the same speed as the rotary motor (i.e., $\Omega \approx \omega$) but in the opposite direction; the flagellum thus becomes "motionless" and the organism would be unable to propel [46].

It is therefore necessary to include a head in the model for a swimming bacterium in a Brinkman medium and enforce the force-free and torque-free conditions [Eqs. (9) and (10)] simultaneously to obtain the induced swimming speed and rotation speed Ω [Eqs. (11) and (12)]. In Fig. 3, we examine how the size of the head affects the swimming speed [Fig. 3(a)] and rotation speed [Fig. 3(b)] for different values of scaled resistance $a\alpha = 0.1$, 1, and 5 (solid lines), compared with the

results in a purely viscous liquid by Chwang and Wu [41] (dashed lines). For a given resistance $a\alpha$, while the induced rotation speed decreases monotonically as the head size increases [Fig. 3(b)], the swimming speed of the bacterium, varies nonmonotonically with the head size [Fig. 3(a)]: The speed first increases with the head size, reaches a maximum value at some optimal head size, and then decreases when the head becomes excessively large. As expected, the speed reduces to zero when the head becomes vanishingly small [Fig. 3(a)], in which case the induced counter-rotation speed becomes as large as the speed driven by the rotary motor $(\Omega/\omega = 1)$ [Fig. 3(b)]. The same trends apply to both swimming in a purely viscous liquid and in a Brinkman medium. However, as the scaled resistance $a\alpha$ increases, the speed of a swimming bacterium indeed decreases consistently for all values of head size as shown in Fig. 3(a); this is in stark contrast to the conclusion for a rotating helix in Sec. III A, where the propulsion speed increases with the resistance $a\alpha$.

To generate more direct comparisons with the results of a rotating helix shown in Fig. 2, we show the corresponding optimal speed of a swimming bacterium as a function of the resistance in Fig. 4. We note that while the speed is optimized over the pitch angle in Fig. 2, the speed is optimized over both the head size and the pitch angle for the full model of a swimming bacterium here. However, even with more extensive optimization, the speed of the swimming bacterium still decreases with increased resistance in the Brinkman medium [Fig. 4(a)]. The corresponding optimal head size and pitch angle are shown in Fig. 4(b). To summarize, while the additional resistance increases the speed of rotating helix driven by an external torque [Fig. 2(a)], the same resistance reduces the speed of a swimming bacterium in a Brinkman medium [Fig. 4(a)]. As a remark, a more complex speed dependence on resistance is observed at much smaller values of resistance (see the Appendix for details).

We further examine the physical origin underlying the qualitatively different speed dependence on the resistance in the two scenarios of helical locomotion (Fig. 2 versus Fig. 4). Compared with the case of a rotating helix driven by an external torque, the presence of a head in a swimming bacterium introduces two major differences: (1) the additional

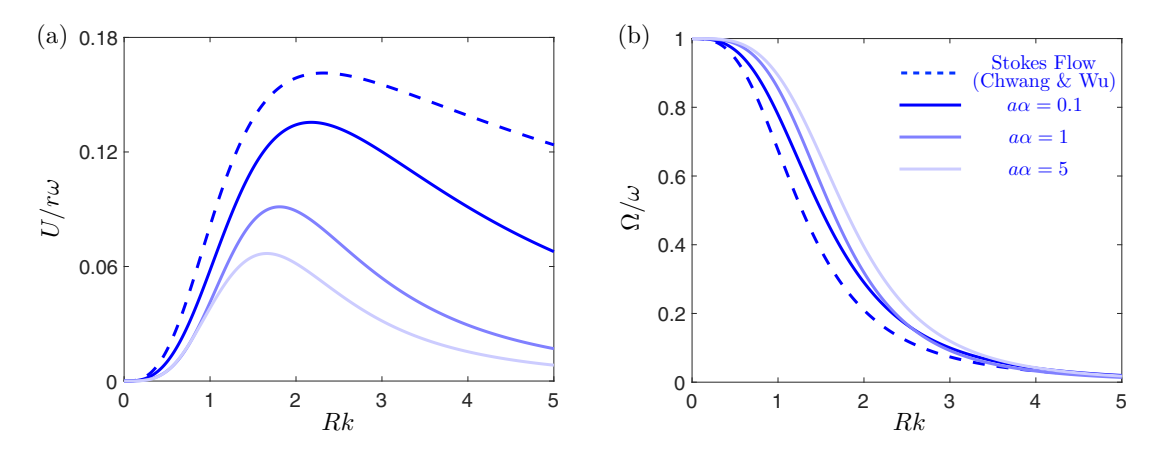


FIG. 3. The effect of the head size on the speed of a swimming bacterium in a Brinkman medium. The variation of (a) the scaled swimming speed, $U/r\omega$, and (b) scaled rotation rate of the head, Ω/ω , as a function of the scaled head size Rk of a swimming bacterium at different values of the scaled resistance $a\alpha$ [see the legend in (b)] at a fixed pitch angle $\theta = \pi/4$ and N = 3. The dashed lines are results in a purely viscous liquid (Stokes flow) by Chwang and Wu [41].

drag caused by the head to the overall structure and (2) the reduced effective rotation velocity of the flagellum due to the induced counter-rotation of the bacterium. We elucidate the crucial roles both effects play in the observed difference in the speed dependence. Through a third relevant scenario of helical locomotion: a cargo-carrying helical propeller driven by an external torque (Sec. III C), we argue that including only the first effect would lead to yet another qualitatively different speed dependence on the resistance. A comparison between the results in this section and the next will reveal the relative importance of the two individual effects in different scenarios.

C. A cargo-carrying helical propeller driven by an external torque

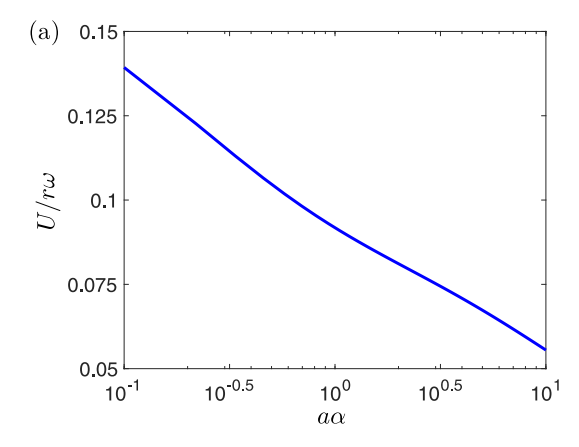
We consider here a relevant scenario of a cargo-carrying helical propeller driven by an external torque. Compared with the two effects due to the head in a swimming bacterium (Sec. III B), the cargo-carrying helical propeller here retains only the first effect of additional drag (due to the presence of the passive cargo) but not the second effect of

counter-rotation. Such a model allows us to examine the speed dependence on the resistance by separating the first and second effects. As a remark, we use the scenario here not only to unravel the two effects due to the presence of a head in a swimming bacterium (Sec. III B) but also as a model for the application of artificial microswimmers in drug delivery applications where the cargo represents a therapeutic payload attached to the propeller [47].

Since the rotating helical propeller with a cargo is externally torqued, we enforce only the force-free condition [Eq. (9)] with the drag from the cargo represented by the term \mathbf{F}_h to obtain the propulsion speed as

$$\frac{U}{r\omega} = \frac{(\gamma - 1)\kappa}{1 + \gamma\kappa^2 + AC_f}.$$
 (15)

Increasing the resistance in a Brinkman medium leads to two competing effects: on one hand, the increased resistance enhances the propulsive thrust generated by the rotating helix through greater drag anisotropy γ in Eq. (15), which tends to increase the propulsion speed; on the other hand, the drag acting on the cargo increases with the resistance in



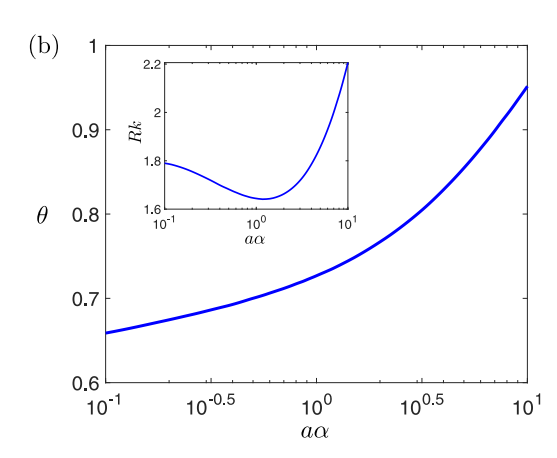


FIG. 4. The effect of resistance in a Brinkman medium on the speed of a swimming bacterium. (a) The scaled swimming speed, $U/r\omega$, as a function of the scaled resistance $a\alpha$. For each value of the scaled resistance, the speed is optimized over both the pitch angle θ and the scaled head size Rk. Here N=3. The corresponding optimal values of θ and Rk are shown in (b) and its inset, respectively.

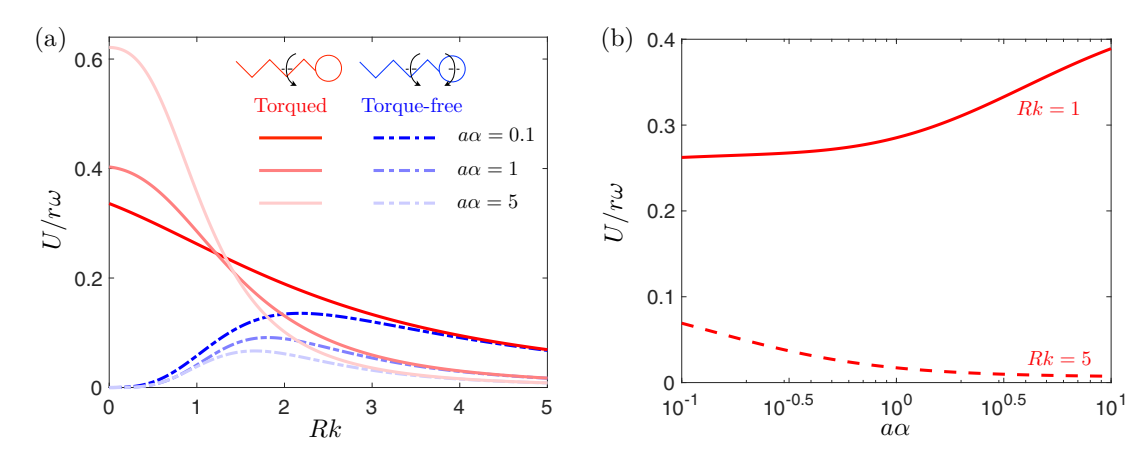


FIG. 5. Propulsion of a cargo-carrying helical propeller driven by an external torque. (a) The scaled propulsion speed, $U/r\omega$, of the torqued propeller as a function of the scaled cargo size Rk at different values of the scaled resistance $a\alpha$ (red solid lines) at a fixed pitch angle $\theta = \pi/4$. For comparison, the speed of a force-free and torque-free swimming bacterium with identical geometrical setup is also shown (blue dot-dashed lines). (b) The dependence of the propulsion speed of a cargo-carrying helical propeller on the scaled resistance $a\alpha$ at a fixed pitch angle $\theta = \pi/4$. Depending on the scaled cargo size Rk, the propulsion speed can either increase (Rk = 1) or decrease (Rk = 5) with the resistance. In all cases considered here, N = 3.

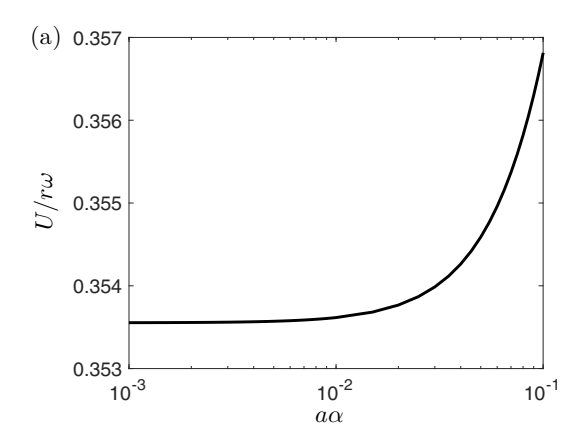
the Brinkman medium through C_f in Eq. (15), which tends to lower the propulsion speed. These two competing effects give rise to two different speed dependencies on the resistance as shown in Fig. 5(a), depending on the cargo size, Rk (red solid lines). When the cargo size is small (e.g., Rk = 1), the increase in drag on the cargo is relatively small compared with the enhancement in propulsive thrust as the resistance α increases. The propulsion speed therefore increases with the resistance $a\alpha$ in this small Rk regime [Fig. 5(b), Rk = 1]. However, as the cargo size becomes sufficiently large (e.g., Rk = 5), the effect due to the increased drag on the cargo becomes eventually more significant than the enhancement in propulsive thrust. In this large Rk regime, the propulsion speed therefore decreases with increased resistance $a\alpha$ [Fig. 5(b), Rk = 5]. Therefore, whether a helical propeller carrying cargo moves faster or slower in a Brinkman medium with increased resistance largely depends on the size of the cargo.

Finally, we contrast the above results with that of a swimming bacterium in Sec. IIIB to highlight the crucial role of the second effect of counter-rotation, which is absent in the case of a cargo-carrying helical propeller. In Fig. 5(a), we contrast the speed dependence on resistance for a swimming bacterium (blue dot-dashed lines) and cargo-carrying helical propeller (red solid lines), for the same size of head and cargo. When the head size is small (e.g., Rk = 1), the second effect due to the counter-rotation of the bacterium causes the speed of the bacterium to decrease with increased resistance (blue dot-dashed lines), opposite to the speed dependence for a cargo-carrying helical propeller (red solid lines). This implies that, for small head sizes, the speed reduction of a swimming bacterium with increased resistance in a Brinkman medium is primarily caused by the second effect, namely the reduction in the apparent rotation speed of the flagellum due to the counter-rotation of the bacterium. On the contrary, as the head size becomes large, the results of a swimming bacterium (blue dot-dashed lines) and a cargo-carrying helical propeller (red solid lines) converge, because the induced counter-rotation becomes insignificant; the speed reduction with increased resistance is thus primarily due to increased drag on the head of the bacterium.

IV. CONCLUDING REMARKS

In this paper, we have extended the previous analysis by Chwang and Wu in a purely viscous liquid [41] to probe the effect of resistance due to a network of stationary obstacles on the swimming of a bacterium in a porous medium. In a local RFT framework, the resistance in a Brinkman medium was previously shown to enhance the propulsion speed of a rotating helix [17]. We have employed the same framework to show that the resistance can, on the contrary, reduce the speed of a swimming bacterium consisting of a helical flagellum and a spherical head. Some estimates of the enhancement and reduction are as follows: based on the estimates in Ref. [17], for a flagellum radius $\approx 0.05 \ \mu m$ swimming in a sparse fiber matrix (0.1% vol) with a fiber radius 1 nm (e.g., polysaccharide chains in the extracellular medium), the scaled resistance $\alpha a \approx 1.5$ was estimated to enhance propulsion of a rotating helical propeller by approximately 40%. Using the same estimate of the scaled resistance, the optimal speed of a swimming bacterium could, instead, drop by more than 50% [Fig. 4(a)]. We have also analyzed a third scenario of a cargocarrying helical propeller to elucidate its difference compared with a swimming bacterium. The qualitatively different speed dependence on resistance in a Brinkman medium highlights the subtle differences between various modes of helical locomotion. We remark that the above conclusions are based on the results in the regime $a\alpha \ge 0.1$, which is relevant to flagellar locomotion in typical filamentous media [17,28,30,44]; the effectiveness of the RFT framework in this regime was validated against numerical simulations that account for the network of stationary obstacles explicitly [17].

We comment on several limitations of the current model. First, the Brinkman medium approach is expected to become less accurate at concentrated porous media [27]. Second, since RFT is a local theory that neglects the hydrodynamic



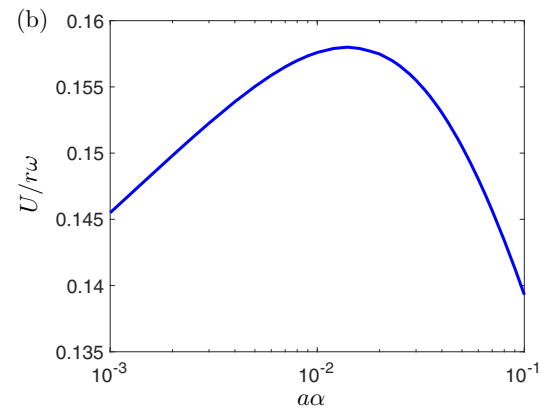


FIG. 6. The scaled speed $U/r\omega$ of (a) a rotating helical propeller driven by an external torque and (b) a swimming bacterium in the regime of small scaled resistance $a\alpha$. The results shown in (a) and (b) above are the corresponding results of Figs. 2(a) and 4(a), respectively, but in the regime where $10^{-3} \le a\alpha \le 10^{-1}$.

interactions between different parts of the filament, we expect the framework to be less accurate for helical geometries with smaller wavelengths, where stronger intrafilament hydrodynamic interactions occur [48]. In addition, the hydrodynamic interaction between the helical flagellum and the cell body is not included in the RFT framework. Results from the current model provide benchmarks for comparisons with future simulations that account for full hydrodynamic interactions and dynamics in more concentrated porous media.

We also remark on the notion of modeling bacterial locomotion in polymeric solutions as locomotion in a network of stationary obstacles formed by entangled linear polymer molecules [17,34,49–51] by interpreting that a higher polymer concentration leads to a larger resistance in the Brinkman medium. The rather substantial decrease in the speed of a swimming bacterium predicted at large values of resistance above is consistent with the measured decrease in swimming speed in polymeric solutions at high polymer concentrations. At low polymer concentrations, in contrast, experiments measured increased bacterial swimming speeds [34,49]. Indeed, such a nonmonotonic speed variation is also captured at very small values of resistance as shown in the Appendix. However, since the current framework is not expected to be quantitatively accurate in the small resistance regime, we only make a cautionary note here and call for subsequent investigations into these observations. Finally, we note that more complex effects, such as the elastic response of the network [21], non-Newtonian rheology [52–54], local viscosity differences [55], and polymer depletion [56,57], may also play important roles in bacterial locomotion in polymeric solutions that are not captured in this paper.

ACKNOWLEDGMENT

Funding support by the National Science Foundation (Grant No. EFMA-1830958 to O.S.P.) is gratefully acknowledged.

APPENDIX: LOCOMOTION IN THE REGIME OF SMALL RESISTANCE

Flagellar locomotion in typical filamentous media is estimated to occur in the regime where $a\alpha \sim O(0.1)$ –O(1) or

higher [17,28,30,44]. Moreover, since the current framework is not expected to be quantitatively accurate for much smaller values of resistance, the results in the main text focus on the regime of $a\alpha \ge 0.1$. For completeness, in this Appendix we remark on some interesting observations on results for much smaller values of resistance.

First, we present the results for a rotating helical propeller driven by an external torque (Sec. III A) in the small resistance regime in Fig. 6(a). The propulsion speed monotonically increases with the scaled resistance in the same way as the results for larger resistance [Fig. 2(a)]. Next, we examine the speed of a swimming bacterium consisting of a helical flagellum and a head (Sec. III B) in the small resistance regime. A more complex speed variation is revealed in this regime: In contrast to the monotonic decay in speed at larger resistance [Fig. 4 (a)], our results suggest that a swimming bacterium could indeed show an increased speed in a porous medium with a very small resistance, before a decrease in speed at larger resistance [Fig. 6(b)].

The nonmonotonic speed variation shown in Fig. 6(b) is qualitatively similar to experimental measurements of bacterial swimming speeds in polymeric solutions [34,49], when the resistance in a porous medium is correlated with the polymer concentration: While a speed enhancement was observed at low polymer concentrations, a more substantial decrease in speed occurred at higher concentrations. Berg and Turner [34] suggested that the observed phenomenon may be attributed to flagellum pushing on the loose and quasirigid networks formed by long linear polymer molecules (e.g., polyvinylpyrrolidone and methylcellulose). Based on this hypothesis, Magariyama and Kudo [50] introduced a phenomenological model with two apparent viscosities to capture the interaction between the swimmer and its surrounding network. While the model predicted similar nonmonotonic behaviors, the physical origin of the phenomenological parameters remain unclear. Our results here are based on a more physical framework [17] developed to model the embedded polymer network in the viscous solution as a porous medium described by the Brinkman equation. Although our model can predict qualitatively similar behaviors as those obtained in the experiment and the phenomenological model, the nonmonotonic behaviors occur in the small resistance regime where the modified force densities may no longer be quantitatively accurate [17]. We therefore only leave a cautionary

remark here and call for further investigations into these observations.

- [1] D. F. Blair, Annu. Rev. Microbiol. 49, 489 (1995).
- [2] K. M. Ottemann and J. F. Miller, Mol. Microbiol. 24, 1109 (1997).
- [3] E. Lauga, Annu. Rev. Fluid Mech. 48, 105 (2016).
- [4] L. J. Fauci and R. Dillon, Annu. Rev. Fluid Mech. 38, 371 (2006).
- [5] E. Lauga and T. R. Powers, Rep. Prog. Phys. 72, 096601 (2009).
- [6] E. M. Purcell, Am. J. Phys. 45, 3 (1977).
- [7] C. Brennen and H. Winet, Annu. Rev. Fluid Mech. **9**, 339 (1977).
- [8] N. Cohen and J. H. Boyle, Contemp. Phys. 51, 103 (2010).
- [9] J. M. Yeomans, D. O. Pushkin, and H. Shum, Eur. Phys. J. Spec. Top. 223, 1771 (2014).
- [10] M. Sitti, Nature 458, 1121 (2009).
- [11] B. J. Nelson, I. K. Kaliakatsos, and J. J. Abbott, Annu. Rev. Biomed. 12, 55 (2010).
- [12] S. Sengupta, M. E. Ibele, and A. Sen, Angew. Chem. Int. Ed. 51, 8434 (2012).
- [13] K. E. Peyer, L. Zhang, and B. J. Nelson, Nanoscale 5, 1259 (2013).
- [14] W. Gao and J. Wang, ACS Nano 8, 3170 (2014).
- [15] J. Katuri, X. Ma, M. M. Stanton, and S. Sánchez, Acc. Chem. Res. 50, 2 (2017).
- [16] A. C. H. Tsang, E. Demir, Y. Ding, and O. S. Pak, Adv. Intell. Syst. 2, 1900137 (2020).
- [17] A. M. Leshansky, Phys. Rev. E 80, 051911 (2009).
- [18] S. A. Mirbagheri and H. C. Fu, Phys. Rev. Lett. 116, 198101 (2016).
- [19] C. Bechinger, R. Di Leonardo, H. Löwen, C. Reichhardt, G. Volpe, and G. Volpe, Rev. Mod. Phys. 88, 045006 (2016).
- [20] Z. Wu, Y. Chen, D. Mukasa, O. S. Pak, and W. Gao, Chem. Soc. Rev. (2020).
- [21] H. C. Fu, V. B. Shenoy, and T. R. Powers, Europhys. Lett. 91, 24002 (2010).
- [22] S. Jung, Phys. Fluids 22, 031903 (2010).
- [23] C. K. W. Tam, J. Fluid Mech. 38, 537 (1969).
- [24] S. Childress, J. Chem. Phys. 56, 2527 (1972).
- [25] I. D. Howells, J. Fluid Mech. 64, 449 (1974).
- [26] E. J. Hinch, J. Fluid Mech. 83, 695 (1977).
- [27] L. Durlofsky and J. F. Brady, Phys. Fluids 30, 3329 (1987).
- [28] N. Ho, S. D. Olson, and K. Leiderman, Phys. Rev. E **93**, 043108 (2016).
- [29] K. Leiderman and S. D. Olson, Phys. Fluids 28, 021902 (2016).
- [30] H. Nganguia and O. S. Pak, J. Fluid Mech. 855, 554 (2018).
- [31] N. Ho, K. Leiderman, and S. Olson, J. Fluid Mech. 864, 1088 (2019).
- [32] H. Nganguia, L. Zhu, D. Palaniappan, and O. S. Pak, Phys. Rev. E. 101, 063105 (2020).
- [33] H. C. Berg and R. A. Anderson, Nature 245, 380 (1973).
- [34] H. C. Berg and L. Turner, Nature **278**, 349 (1979).

- [35] A. Ghosh and P. Fischer, Nano Lett. 9, 2243 (2009).
- [36] L. Zhang, J. J. Abbott, L. Dong, B. E. Kratochvil, D. Bell, and B. J. Nelson, Appl. Phys. Lett. 94, 064107 (2009).
- [37] L. Zhang, J. J. Abbott, L. Dong, K. E. Peyer, B. E. Kratochvil, H. Zhang, C. Bergeles, and B. J. Nelson, Nano Lett. 9, 3663 (2009)
- [38] L. Zhang, K. E. Peyer, and B. J. Nelson, Lab Chip **10**, 2203 (2010).
- [39] I. Gibbons, J. Cell Biol. **91**, 107s (1981).
- [40] D. K. Vig and C. W. Wolgemuth, Phys. Rev. Lett. 109, 218104 (2012)
- [41] A. Chwang and T. Y. Wu, Proc. R. Soc. London, Ser. B 178, 327 (1971).
- [42] J. Keller and S. Rubinow, Biophys. J. 16, 151 (1976).
- [43] L. Spielman and S. L. Goren, Environ. Sci. Technol. 2, 279 (1968).
- [44] W. Saltzman, M. Radomsky, K. Whaley, and R. Cone, Biophys. J. 66, 508 (1994).
- [45] Y. E. Solomentsev and J. L. Anderson, Phys. Fluids 8, 1119 (1996).
- [46] The inclusion of the torque due to the spinning motion of the filament would lead to a negligibly small but finite swimming speed when the head size becomes zero. The resulting swimming speed scales quadratically with the filament radius as $U/c = O(a/r)^2$, which is practically zero due to the slenderness of biological filaments in flagellar locomotion as elucidated by Chwang and Wu [41]. We therefore do not include the torque due to the spinning motion of the filament in our analysis.
- [47] W. Gao, D. Kagan, O. S. Pak, C. Clawson, S. Campuzano, E. Chuluun-Erdene, E. Shipton, E. E. Fullerton, L. Zhang, E. Lauga, and J. Wang, Small 8, 460 (2012).
- [48] B. Rodenborn, C.-H. Chen, H. L. Swinney, B. Liu, and H. P. Zhang, Proc. Natl. Acad. Sci. USA 110, E338 (2013).
- [49] W. R. Schneider and R. N. Doetsch, J. Bacteriol. 117, 696 (1974).
- [50] Y. Magariyama and S. Kudo, Biophys. J. 83, 733 (2002).
- [51] A. E. Patteson, A. Gopinath, M. Goulian, and P. E. Arratia, Sci. Rep. 5, 15761 (2015).
- [52] B. Liu, T. R. Powers, and K. S. Breuer, Proc. Natl. Acad. Sci. 812, R3 (2011).
- [53] S. E. Spagnolie, B. Liu, and T. R. Powers, Phys. Rev. Lett. 111, 068101 (2013).
- [54] S. Gómez, F. A. Godínez, E. Lauga, and R. Zenit, J. Fluid Mech. 812 (2017).
- [55] V. A. Martinez, J. Schwarz-Linek, M. Reufer, L. G. Wilson, A. N. Morozov, and W. C. K. Poon, Proc. Natl. Acad. Sci. 111, 17771 (2014).
- [56] Y. Man and E. Lauga, Phys. Rev. E 92, 023004 (2015).
- [57] A. Zottl and J. Yeomans, Nat. Phys 15, 554 (2019).